JOURNAL OF NANO- AND ELECTRONIC PHYSICS
Vol. **17** No 4, 04004(7pp) (2025)

ЖУРНАЛ НАНО- ТА ЕЛЕКТРОННОЇ ФІЗИКИ
Том **17** № 4, 04004(7cc) (2025)

OPEN ACCESS

REGULAR ARTICLE

Morphological and Optical Properties of Silicon Micro-nanostructures Induced by DC Corona Discharge at Atmospheric Pressure

O. Boudia[1,2], F. Bitam-Megherbi[1,2,*] ✉, M. Mekious[1,2], F. Bouaraba[1,2], M. Megherbi[1]

[1] *Advanced Technologies Laboratory for Electrical Engineering, Tizi-Ouzou, Algeria*
[2] *Mouloud Mammeri University of Tizi-Ouzou, Algeria*

(Received 19 June 2025; revised manuscript received 21 August 2025; published online 29 August 2025)

In this work, the progressive evolution of silicon surface micro-nanostructures was demonstrated using a DC negative corona discharge at atmospheric pressure in ambient air. The morphologies of textured multicrystalline silicon (mc-Si) and monocrystalline silicon (c-Si) wafers were observed using scanning electron microscopy. It was found that, with increasing treatment duration under corona discharge, various microstructures were formed, such as microspheres on the mc-Si wafer and microspikes with spherical tips on the c-Si wafer. The surface reflectance of the fabricated microstructures was studied using a UV-VIS spectrophotometer. The results showed that the light-trapping effect was significantly enhanced by the microstructures produced during corona plasma treatment, leading to a substantial reduction in light reflectance. The surface reflectivity in the wavelength range of 200 nm to 1000 nm was found to be less than 8 % for the textured mc-Si and as low as 0.78 % for the textured c-Si. Additionally, the photoluminescence properties of the microstructures revealed a red shift in the emission peaks. This effect could be beneficial for the development of silicon-based photovoltaic cells, optoelectronic devices, and luminescent applications.

Keywords: Silicon, Surface microstructures morphology, Corona discharge, Reflectivity, Optical properties.

DOI: 10.21272/jnep.17(4).04004 PACS numbers: 71.20.Mq, 73.40.Ty, 78.66.Fd

1. INTRODUCTION

Silicon has been widely studied due to its abundant reserves [1, 2], low cost and toxicity [3], and high thermal stability [4], making it a promising candidate for a wide range of applications including solar cells, light emitting devices, semiconductor components (diodes, transistors, integrated circuits), and sensor [5-7]. However, with an indirect band gap (1.12 eV), silicon has limited potential for optoelectronics application [8-10], additionally, its surface reflects 30-40 % of incident light in the visible and near-infrared spectral range where it is photosensitive [11-13].

The antireflective properties of the silicon surface directly impact the performance of many optoelectronic applications, including solar cells. To reduce unwanted reflections and enhance light absorption, researchers have developed various techniques. One approach is to deposit antireflective coating (ARC) layers on the sili-con surface [14-15]. Traditionally, antireflection (AR) is achieved using single layer coating such as: SiO_2, SiC, and SiN_x [16-17]. However, the antireflective properties of these coatings are limited to a narrow wavelength range of the spectrum. In contrast, double or triple layer coatings, such as SiO_2/SiN_x and $SiO_x/SiO_xN/SiC/SiN_x$ [18, 19], provide more effective AR property over a broader range of wavelengths [20]. Although single layer antireflection coatings with textured surface are commonly used in industrial production, they require deposition techniques such as PECVD for SiN coatings. On the other hand, multi-layered AR coatings face challenges related to the availability of cost effective materials with suitable refractive indices and compatible thermal expansion coefficients [13].

The fabrication of micro and nanostructures on silicon surface has proven to be an effective way to overcome these limitations. Silicon micro and nanostructures have attracted significant experimental and theoretical interest due to their high absorption efficiency across a wide wavelength range (200-2500 nm) [21-22]. Light trapping in these structures is achieved by extending the optical path through multiple reflections and by energy attenuation resulting from the interaction between light and the silicon material [23]. Many efforts have been dedicated to reducing reflection by applying micro or nano structures to the silicon surface such as microspikes, microgrooves, microcones, nanoripples, nanowires, nanoholes [24] among others. To date, several approaches can be used to obtain desired micro/nanostructures on the silicon surface such as Metal Assisted Chemical Etching (MACE), Reactive Ion Etching (RIE), plasma etching, and laser induced texturing

* Correspondence e-mail: ferroudja.bitammegherbi@ummto.dz

Cite this article as: O. Boudia et al., *J. Nano- Electron. Phys.* 17 No 4, 04004 (2025) https://doi.org/10.21272/jnep.17(4).04004

[4, 25-28]. As for mentioned, MACE has the potential to produce high AR structures and large scale micro/nanostructures. In MACE Silicon etching is guided by a metal layer (which is often a noble metal such as Pd, Ag or Au) that catalyzes the local dissolution of silicon in the presence of fluoride ions and oxidation in an etchant solution [29-31]. However, this method is tedious and involves the use of hazardous etchants (e.g., HF). This technology utilizes noble metals, which can act as deep traps for photo-carriers, leading to a decrease in solar cell performance [32, 33]. Reactive Ion Etching (RIE) or ion-assisted plasma etching is a widely used technique for etching silicon surfaces with plasma assistance and a chemical etch component [34]. RIE is highly anisotropic [35], allowing for better resolution compared to wet chemical etching [36]. The first step in this process is selecting suitable plasma. Fluorine-based and chlorine-based gases are typically used, with several fluorine-based gases such as CHF_3 and SF_6, O_2 as an oxidizing gas, and H_2 as a reducing gas [37, 38]. However, this process is usually complex and requires a high level of maintenance.

In the last few years, laser processing has been demonstrated as a promising approach due to its flexibility, simplicity, and controllability in creating various types of micro-nanostructures [39]. The evolution of micro-nanostructures in monocrystalline silicon following pulsed laser irradiation significantly affects its mechanical and electrical properties [26]. Highly absorptive silicon, known as black silicon, was developed by structuring silicon through laser processing in different background environments [40]. The morphology of the silicon surface during pulsed laser interaction depends on the background environment (gas or liquid) [41, 42]. The resulting micro-nanostructures tend to be sharper in the presence of gaseous reactants such as SF_6, Cl2, and SiH4. M.A. Sheely et al. analyzed the role of background gas in determining the morphology and optical properties of a silicon surface irradiated with a train of femtosecond laser pulses in the presence of SF_6, H_2, SiH_4, and a mixture of Ar and SF_6. They showed that the presence of sulfur (S) in these gases plays a key role in creating sharp micro-nanostructures [43]. The laser parameters, including laser intensity, pulse duration, wavelength, and pulse width (femto-, pico-, nanosecond, CW, UV…), and laser fluence, are also important factors in controlling the properties of laser-induced surface structures [25, 44]. For example, Peng et al. studied the effect of laser wavelength on the formation of silicon microstructures and found that by varying the laser wavelength and pulse number, the morphology of the fabricated microstructures could be controlled [21]. Nayak et al. investigated the origin and evolution of self-organized conical micro/nanostructures on the silicon surface after irradiation with multiple ultrafast femtosecond laser pulses in gaseous environments of SF6 and He [45]. Skantzakis et al. explored the effect of laser pulse duration on the morphology of microcones produced by UV laser irradiation in an SF_6 environment [46]. Their results revealed a strong correlation between the morphological characteristics and laser parameters, including pulse duration, laser fluence, and the number of pulses. Laser surface modification results from reactions under extreme conditions that cause rapid localized heating and cooling in the excited region. Laser irradiation thus serves as a means of energy deposition into materials, inducing extremely high temperatures and pressures, which can lead to surface and subsurface defects such as dislocations and lattice distortions [47-49]. As mentioned earlier, shaping surfaces through pulsed laser ablation has emerged as a competitive alternative to wet etching. However, the physical processes involved strongly depend on various factors, including irradiation conditions, ambient conditions [50, 51], and the processing environment (liquid, gas, or vacuum) [52]. Atmospheric pressure gas discharge plasmas, especially those operating in energy non-equilibrium and at low temperatures, have recently attracted great interest for a wide range of technologies, including surface treatment, activation, functionalization, etching, and thin-film deposition [53]. Discharges at atmospheric pressure allow substrate materials to be exposed to plasma without the need for expensive vacuum equipment. The main advantage is that materials can be treated continuously and in real-time at ambient temperature [54]. The treatment of silicon surfaces using cold atmospheric plasma (CAP) has attracted significant attention due to its ability to effectively modify surface properties. CAP can enhance the structural, optical, and electrical characteristics of silicon materials, making it suitable for various applications [55]. Silicon micro-nanostructures can be synthesized and modified using cold plasma techniques at atmospheric pressure [56]. Various methods, including cold atmospheric pressure plasma jets and micro-arc techniques, have demonstrated the ability to manipulate the properties of silicon micro-nanostructures. Pokryshkin et al. showed that the use of helium and argon plasma jets (CAP jets) led to significant modifications in silicon nanowires (Si-NWs), including changes in length and sharpness. The treatment also resulted in increased silicon oxide formation and altered electrical properties [55]. The Helix Jets, a plasma source operating at atmospheric pressure with RF power and a gas mixture (Ar, He, SiH_4), was used for the synthesis of silicon nanoparticles (Si-NPs) [57]. Silicon nanostructures were also synthesized using a DC atmospheric pressure microplasma jet with an $Ar/SiH_4/H_2$ gas mixture, demonstrating an effective method for producing nanomaterials under atmospheric conditions [58]. Plasma suitable for cleaning and activation has to be non-equilibrium and low temperature one, to allow for rapid processing times and reduced costs compared to the traditional low pressure treatment [58]. The most popular cold atmospheric plasma sources are based on DBD (Dielectric Barrier Discharges). DBD generates non-equilibrium, low-temperature plasma at atmospheric pressure, characterized by filamentary micro-discharges [53]. This method uses atmospheric pressure plasma to

modify silicon surfaces, significantly increasing surface energy, which improves wettability [59, 60] and reduces contamination. DBD cleans silicon surfaces by removing contaminants, with studies showing a substantial decrease in ions such as Na^+ and K^+ after plasma treatment. Beyond cleaning, plasma treatment also enhances the adhesion of nanoparticles, such as gold, to the silicon surface and results in a smoother surface morphology, which is beneficial for subsequent applications in microelectronics [61]. Additionally, the process can be adapted for etching silicon dioxide layers, enabling precise surface preparation without the need for harsh chemicals [62].

Corona discharge systems are another method for generating cold atmospheric pressure plasma. This occurs when a neutral gas is ionized by an external electric field [63]. Corona discharges exist in several forms, depending on the polarity of the field and the electrode's geometrical configuration. In the case of negative corona using a point-plate electrode configuration (where the point is connected to the negative terminal of the power supply), the initial form is Trichel pulse corona, followed by pulseless corona and eventually spark discharge as the applied voltage increases. Negative corona discharge generally propagates through impact ionization of gas molecules [64]. The use of corona discharge for surface modification was reported by Zanet et al. [65]. Their studies indicated that corona treatment can modify the surface texturing of silicon carbide (SiC) and alter surface roughness, which is crucial for light absorption in photovoltaic cells and for improving the interface in microelectronic devices.

To the best of our knowledge, no work has been published on the use of corona plasma for fabricating silicon micro-nanostructures to enhance light trapping on silicon surfaces. In this study, micro-nanostructures were fabricated using a DC negative corona discharge at atmospheric pressure in ambient air. We examined how treatment duration impacts surface morphology and optical properties, highlighting its influence on the final structures.

2. EXPERIMENTAL DETAILS

2.1 Sample Preparation

Two types of silicon were used in our experiment: *n*-type monocrystalline silicon (c-Si) (100) Czochralski with a resistivity of 100 Ω·cm and a thickness of 400 μm, and *p*-type multicrystalline silicon (mc-Si) with a resistivity of 1.5 Ω·cm and a thickness of 450 μm. The silicon substrates, measuring 10 mm × 10 mm, were first cleaned with acetone for 10 minutes, followed by deionized water to remove surface contamination. They were then immersed in diluted hydrofluoric acid (HF, ~ 10 %) to eliminate the native oxide layer.

2.2 Corona Discharge Reactor

The corona discharge reactor is mainly composed of a pointed electrode and a planar electrode, both made of stainless steel. The pointed electrode has an opening angle of 30°, while the planar electrode has a diameter of 100 mm. The inter-electrode distance is 20 mm. These electrodes are placed inside a discharge tube to prevent any contamination of the silicon samples during processing. The corona discharge, generated at atmospheric pressure, operates at a voltage of 23 kV. A photograph of the experimental setup is shown in Fig. 1.

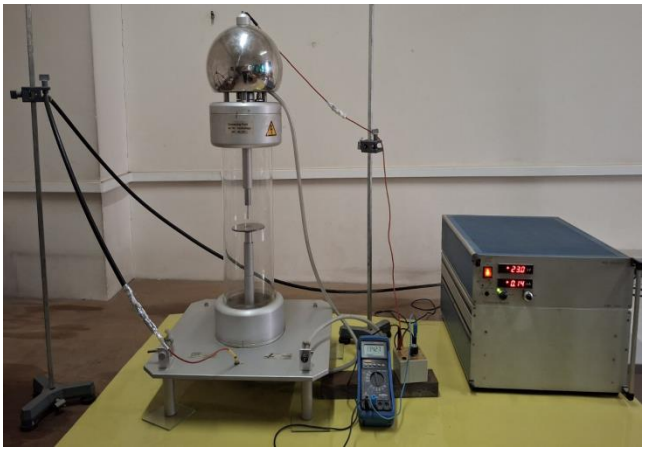

Fig. 1 – Photograph of experimental setup

2.3 Procedure for Sample Treatment

To investigate the effect of corona discharge on the silicon surface, monocrystalline silicon (c-Si) samples (Simono1, Simono2, Simono3, and Simono4) were treated with negative corona discharge for 2, 4, 6, and 8 hours, respectively. Multicrystalline silicon (mc-Si) samples (Simc1, Simc2, and Simc3) underwent the same treatment for 2, 4, and 6 hours, respectively. A Scanning Electron Microscope (SEM) was used to analyze the micro-nanostructures formed after corona treatment. Reflectance spectra were recorded using a UV-VIS spectrophotometer, while photoluminescence spectra were measured at room temperature using an InGaAs laser (375 nm, 100 mW) as the excitation source.

3. RESULTS AND DISCUSSION

3.1 Morphological Properties

The scanning electron microscopy (SEM) results of the fabricated micro-nanostructures on mc-Si samples are summarized in Fig. 1. Figs. 1(a)-1(c) show the typical SEM morphology of mc-Si samples (Simc1, Simc2, and Simc3) after exposure to negative corona plasma for 2, 4, and 6 hours, respectively.

As observed in Fig. 1(a), at a shorter exposure time (2 hours), isolated microspheres (~ 1 μm in size) form on the silicon surface. As the exposure time increases to 4 and 6 hours, as shown in Figs. 1(b) and 1(c), these microspheres gradually evolve into nanoclusters with particle sizes around 500 nm. Some of these clusters merge, forming interconnected nanostructures with

a noticeable reduction in inter-cluster separation (highlighted in the red circle in Fig. 1(c)). Interestingly, the morphology of the micro-nanostructures formed after 6 hours of corona discharge exposure, depicted in Fig. 1(c), suggests that treatment duration is a crucial factor in achieving a uniform distribution of silicon micro-nanostructures.

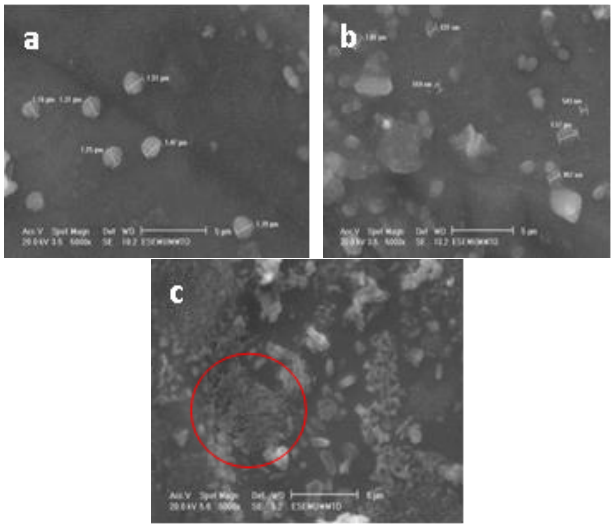

Fig. 2 – SEM pictures of micro-nanostructures formed on the mc-Si samples after corona treatment at exposure time:(a) 2h, (b) 4h, (c) 6h

Fig. 3 illustrates the progressive evolution of silicon surface microstructures in c-Si samples (Simono1, Simono2, Simono3, and Simono4) treated with negative corona plasma for 2, 4, 6, and 8 hours, respectively. As shown in Fig. 3, the silicon microstructures undergo a gradual transformation as the exposure time increases.

Figs. 3(a) and 3(b) show the morphology of the silicon surface after 2 hours of corona treatment, leading to the formation of a non-homogeneous distribution of micro-agglomerates with particle sizes ranging from 3 μm to 5 μm. The cavities between individual agglomerates (indicated by the red arrow) determine the degree of open porosity formed on the surface.

Fig. 3(c) presents a lateral view of the sample treated for 4 hours, where improved homogeneity is observed. The structures grown on the silicon surface exhibit a cauliflower-like morphology (Fig. 3(d)), com-posed of interconnected nanoclusters (red circle). An increased accretion of microstructures into clusters is also noticeable.

As the exposure time to corona discharge increases, the cavity size decreases, and the agglomerates become more uniformly distributed in both parallel and perpendicular orientations relative to the surface (Figs. 3(e) and 3(f)).

The SEM images show that the silicon surface microstructured after 8 hours of processing exhibits the sharpest features, indicating the most intense reaction process, which aligns with the plasma reaction intensity.

Figs. 3(e) and 3(f) illustrate the formation of microspikes on the silicon surface after 8 hours of treatment. These spikes have a conical shape with a spherical tip, suggesting that they were formed by melted silicon that rapidly resolidified.

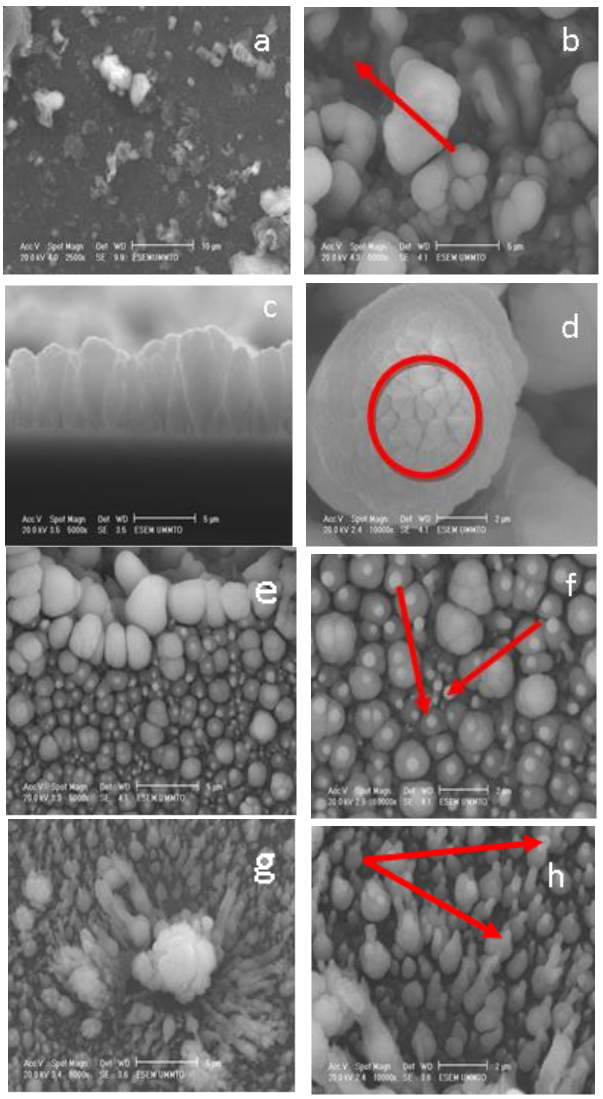

Fig. 3 – SEM pictures of silicon micro/ nanostructures obtained after treatment of: a) 2 hours, b) 4 hours, c) 6 hours and d) 8hours

The formation of spikes on the silicon surface is an iterative process driven by the simultaneous action of physical surface deformation mechanisms such as melting, evaporation, and etching. The effectiveness of each mechanism in this complex surface reshaping process depends on the processing duration. A similar structure has been observed on silicon surfaces treated with lasers, as reported in [22]. The micro-nanostructures fabricated using corona discharge suggests that treatment time plays a crucial role in shaping the surface morphology. Longer exposure allows ions and radicals generated by the corona discharge to interact more extensively with the surface, leading to the formation of nanostructures without the need for metallic catalysts or precursors.

3.2 Optical Properties

The antireflection properties of the micronanostructures formed on the two types of silicon used in this study were analyzed using an uvvis spectrophotometer. The reflectance (r) was measured as a function of wavelength (λ) in the range of 200-1000 nm, as shown in Fig. 4. The micro-nanostructures produced during the corona plasma process influence the reflectance properties of silicon, as evident from the reflectance curve. Fig. 4(a) shows that the reflectance of mc-si samples initially decreases and then increases with increasing wavelength. The surface reflectivity dropped from 10 % for the sample treated for 4 hours to 8 % for the one treated for 6 hours. This variation can be attributed to the non-uniformity of the microstructures formed during plasma processing.

The reflectance spectra of the c-si sample surfaces are shown in Fig. 4(b), revealing a further reduction in reflection losses compared to the mc-si samples. The optical reflectivity of all samples gradually decreases across the entire measured spectrum. The sample with micro spikes (simono4) exhibits the lowest reflectance, dropping below 0.78 %. This reduction can be attributed to the enhanced broadband light absorption capabilities of the micro-nanostructures formed during the process, acting as effective light-trapping centers, as depicted in Fig. 3(f). The voids between the micro spikes allow more light to penetrate through their sidewalls, further enhancing light trapping. These microstructures, with their excellent antireflection properties, present strong potential for solar cell applications.

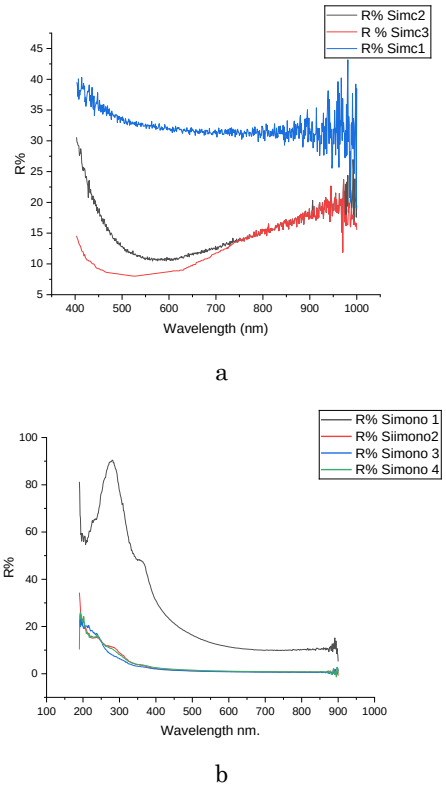

Fig. 4 – Reflectance spectra of micro-nanostructures obtained at different exposure time

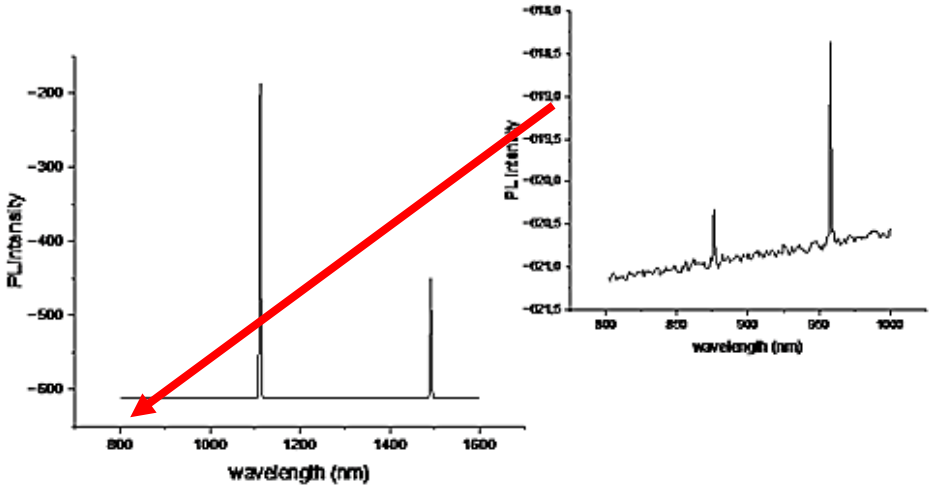

Fig. 5 – Reflectance spectra of micro-nanostructures obtained at different exposure time

After measuring the reflectance properties, we conducted photoluminescence studies on the samples using an InGaAs laser (375 nm, 100 mW) at room temperature. Figure 5 shows the PL spectra of the c-Si samples, revealing a PL peak at $\lambda \approx 1100$ nm and a less intense peak at $\lambda \approx 1500$ nm. A red shift is observed, likely due to additional light-emitting centers of radiative nature.

According to the study reported in reference [66], ion implantation and electron irradiation create defects such as vacancies, which can act as radiative centers and enhance photoluminescence. In our work, the silicon surface was treated with corona plasma in ambient air, and the oxidizing effect of corona discharge is well known. Therefore, the PL emission at red wavelengths is likely caused by defects arising from ion irradiation in the SiO_2/Si system [67, 68].

4. CONCLUSION

This study investigates the evolution of micro- and nanostructures fabricated on two types of silicon surfaces of P-type multicrystalline silicon (mc-Si) and N-type monocrystalline silicon (c-Si) using a DC negative corona discharge generated at atmospheric pressure in ambient air.

The interaction between corona discharge and the silicon surface was examined to understand how the formation of micro- and nanostructures effectively enhances antireflection properties through a cost-effective, simple, and scalable corona discharge texturing method. The findings reveal that the formation of these structures during corona discharge–silicon interaction is strongly influenced by the treatment duration (exposure time). The silicon surface undergoes a progressive transformation, with the micro- and nanostructures evolving as exposure time increases.

Corona discharge-surface interactions result in various micro and nanostructures that significantly enhance light trapping and absorption. On mc-Si surfaces, agglomerated nanoparticles form with increasing exposure time to corona discharge leading to an average reflectance of less than 8% in the visible range.

For c-Si surfaces, exposure time plays a crucial role in surface texturing under cold corona plasma, leading to the formation of conical spikes with spherical tips. These microstructures exhibit outstanding antireflection performance, achieving an ultralow reflectance of less than 0.78 % over the 200-1000 nm wavelength range.

The photoluminescence (PL) properties of the fabricated microstructures reveal a redshift in emission peaks. A maximum PL emission line was observed at $\lambda \approx 1100$ nm, likely due to defects induced by the oxidizing effect of the corona discharge.

The findings of this study provide new insights into light trapping mechanisms, with promising applications in photovoltaics and optoelectronics.

REFERENCES

1. R. Bhujel, S. Rai, U. Deka, J. Biswas, B.P. Swain, *J. Nano-Electron. Phys.* **13** No 2, 02003 (2021).
2. J. Wu, Y. Huang, T. Shang, F. Wang, G. Deng, X. Sui, S. Zhou, *Opt. Mater.* **145**, 114453 (2023).
3. A. Tahhana, Z. Dehouchea, T. Ansonb, G. Fernc, *40th Photovoltaic Specialist Conference* (PVSC), 1296 (IEEE: 2014).
4. J. Salazar, M. Sánchez, A. Aragón, P. Roquero, J.E. Romero, C. Ramos, E. Ramos, A. Dutt, G. Santana, *Mater. Lett.* **377**, 137332 (2024).
5. Y. Ma, J. Si, X. Sun, T. Chen, X. Hou, *Appl. Surf. Sci.* **313**, 905 (2014).
6. X.B. Guo, J.-N. Ding, S.Y. Wang, J.H. Qiu, B. Kan, N.-Y. Yuan, 8th *Annual IEEE International Conference on Nano/Micro Engineered and Molecular Systems* (NEMS 2013), art. No 6559938, 1218 (SUZHU, China: 2013).
7. L. Zhang, H. Shen, Z. Yue, W. Wang, Y. Jiang, *Appl. Surf. Sci.* **280**, 446 (2013).
8. X. Lu, K. Wu, H. Wu, W. Cao, Q. Zhu, J. Zhou, Y. Zhang, *Opt. Mater.* **137**, 113549 (2023).
9. F. Delachat, M. Carrada, G. Ferblantier, A. Slaoui, C. Bonafos, S. Schamm, H. Rinnert, *Physica E* **41** No 6, 994 (2009).
10. A. Nikolskaya, D. Korolev, A. Mikhaylov, A. Konakov, A. Okhapkin, S. Kraev, A. Sushkov, D. Pavlov, D. Tetelbaum, *Mater. Lett.* **342**, 134302 (2023).
11. A. Ali, M.S. Hussain, R.S. Almufarij, M.Y. Ali, L.G. Alharbe, H.H. Somaily, E.A. Shokralla, S.H. Alrefaee, A. Ashfaq, A.R. Abd-Elwahed, *Ceram. Int.* **50** No 11, 19424 (2024).
12. R. Rebigan, A. Avram, F. Craciunoiu, R. Tomescu, E. Budianu, M. Purica, M. Popescu, *International Semiconductor Conference* (CAS 2013), art. No 668816, 119 (Sinaia, Roumania: 2013).
13. P. Prathap, A.S. Dahiya, M. Srivastava, S.K. Srivastava, B. Sivaiah, D. Haranath, R. Srivastava, C.M.S. Rauthan, P.K. Singh, *Sol. Energy* **106**, 102 (2014).
14. B.T. Chan, E. Kunnen, K. Xu, W. Boullart, J. Poortmans, *IEEE J. Photovolt.* **3** No 1, 152 (2012).
15. M. Halbwax, T. Sarnet, P. Delaporte, M. Sentis, H. Etienne, F. Torregrosa, V. Vervisch, I. Perichaud, S. Martinuzzi, *Thin Solid Films* **516** No 20, 6791 (2008).
16. C.P. Liu, M.W. Chang, C.L. Chuang, *Curr. Appl. Phys.* **14** No 5, 653 (2014).
17. J.A. Silva, S. Quoizola, E. Hernandez, L. Thomas, F. Massines, *Surf. Coat. Technol.* **242**, 157 (2014).
18. T.-W. Kuo, N.-F. Wang, Y.-Z. Tsai, P.-K. Hung, M.-P. Houng, *Mater. Sci. Semicond. Proc.* **25**, 211 (2014).
19. A. Kumar, A. Sharma, A. Agarwal, *IOP Conf. Ser.: Mater. Sci. Eng.* **594**, 012001 (2019).
20. J. Wu, J. Tu, L. Li, X. Xiao, K. Hu, S. Yu, Y. Xie, Y. Yang, H. Wu, *Surf. Interface.* **30**, 101918 (2022).
21. Y. Peng, H. Chen, C. Zhu, D. Zhang, Y. Zhou, H. Xiang, B. Cai, Y. Zhu, *Mater. Lett.* **83**, 127 (2012).
22. S. Liu, J. Zhu, Y. Liu, L. Zhao, *Mater. Lett.* **62** No 23, 3881 (2008).
23. H. Liu, Y. Du, X. Yin, M. Bai, W. Liu, *J. Nanomater.* **2022** No 1, 8139174 (2022).
24. W. Chen, J. Tao, H. Xu, D. Gao, J. Lv, Y. Qin, G. Guo, X. Li, Q. Wang, Z. An, *Res. Phys.* **32**, 105133 (2022).
25. A. Kuriakose, P. Malik, J.N. Acharyya, D. Kalyanasundaram, P. Srivastava, G.V. Prakash, *Opt. Laser Technol.* **179**, 111337 (2024).
26. B.G. Rasheed, M.A. Ibrahem, *Micron* **140**, 102958 (2021).
27. T. Allen, J. Bullock, A. Cuevas, S. Baker-Finch, F. Karouta, 40th *Photovoltaic Specialist Conference* (PVSC), art. No 6924983, 0562 (Denver, USA: 2014).
28. Q. Wang, W. Zhou, *Opt. Mater.* **72**, 508 (2017).
29. H. Ohlin, T. Frisk, I. Sychugov, U. Vogt, *Micro Nano Eng.* **19**, 100178 (2023).
30. H. Alhmoud, D. Brodoceanu, R. Elnathan, T. Kraus, N.H. Voelcker, *Prog. Mater. Sci.* **116**, 100636 (2021).
31. A.K. Behera, R.N. Viswanath, C. Lakshmanan, T. Mathews, M. Kamruddin, *Nano- Struct. Nano-Object.* **21**, 100424 (2020).
32. J. Cao, X. Shen, Z. Yu, J. Zheng, *Mater. Chem. Phys.* **248**, 122909 (2020).
33. H. Lv, H. Shen, Y. Jiang, C. Gao, H. Zhao, J. Yuan, *Appl. Surf. Sci.* **258** No 14, 5451 (2012).
34. E. Oliveira, J. Strassner, C. Doering, H. Fouckhardt, *Appl. Surf. Sci.* **611**, 155769 (2023).
35. Y.X. Li, M.R. Wolffenbuttel, P.J. French, M. Laros, P.M. Sarro, R.F. Wolffenbuttel, *Sensor. Actuat. A: Phys.* **41** No 1-3, 317 (1994).
36. G. Zhao, X. Zhao, H. Zhang, Z. Lian, Y. Zhao, A. Ming,

Y. Lin, *Heliyon* **9** No 12 (2023).
37. T. He, Z. Wang, F. Zhong, H. Fang, P. Wang, W. Hu, *Adv. Mater. Technol.* **4** No 8, 1900064 (2019).
38. J.-Y. Choi, C.B. Honsberg, *39th Photovoltaic Specialists Conference (PVSC)*, art. No 6744355, 1199 (2013).
39. Q. Tan, F. Lu, C. Xue, W. Zhang, L. Lin, J. Xiong, *Sensor. Actuat. A: Phys.* **295**, 560 (2019).
40. A.Y. Vorobyev, C. Guo, *Appl. Surf. Sci.* **257** No 16, 7291 (2011).
41. H.D. Yang, X.H. Li, G.Q. Li, C. Wen, R. Qiu, W.H. Huang, J.-B. Wang, *Appl. Phys. A* **104** No 2, 749 (2011).
42. J.-H. Zhao, X.-B. Li, Q.-D. Chen, Z.-G. Chen, H.-B. Sun, *Mater. Today Nano* **11**, 100078 (2020).
43. M.A. Sheehy, L. Winston, J.E. Carey, C.M. Friend, E. Mazur, *Chem. Mater.* **17** No 14, 3582 (2005).
44. S. Li, X. Wang, G. Chen, Z. Wang, *Micromachines* **14** No 1, 119 (2022).
45. B.K. Nayak, M.C. Gupta, *Opt. Laser. Eng.* **48** No 10, 966 (2010).
46. E. Skantzakis, V. Zorba, D.G. Papazoglou, I. Zergioti, C. Fotakis, *Appl. Surf. Sci.* **252** No 13, 4462 (2006).
47. J. Xie, J. Yan, D. Zhu, G. He, *Adv. Funct. Mater.* **32** No 15, 2108802 (2022).
48. Y. Liu, Y. Ding, J. Xie, L. Xu, I.W. Jeong, L. Yang, *Mater. Design* **225**, 111443 (2023).
49. Y. Liu, Y. Ding, J. Xie, M. Chen, L. Yang, X. Lv, J. Yuan, *Materials* **15** No 14, 4897 (2022).
50. U. Teubner, A. Andreev, V. Makin, J. Imgrunt, *J. Phys. Commun.* **6** No 11, 115003 (2022).
51. S. Besner, J.-Y. Degorce, A.V. Kabashin, M. Meunier, *Photonics North* 2004: *Photonic Applications in Astronomy, Biomedicine, Imaging, Materials Processing, and Education (SPIE, 2004)*, art. No 567746, 554 (Bellingham, WA: 2004).
52. T.-Y. Derrien, R. Koter, J. Krüger, S. Höhm, A. Rosenfeld, J. Bonse, *J. Appl. Phys.* **116** No 7 074902 (2014).
53. L. Bárdos, H. Baránková, *Thin Solid Films* **518** No 23, 6705 (2010).
54. S. Martin, F. Massines, N. Gherardi, C. Jimenez, *Surf. Coat. Technol.* **177**, 693 (2004).
55. N.S. Pokryshkin, V.G. Yakunin, A.I. Efimova, A.A. Elyseev, D.E. Presnov, V.P. Savinov, V.Y. Timoshenko, *Eur. Chem.-Technol. J.* **25** No 2, 73 (2023).
56. M. Dworschak, N. Kohlmann, F. Matějka, P. Galář, L. Kienle, J. Schäfer, J. Benedikt, *Plasma Proc. Polym.* **20** No 2, 2200129 (2023).
57. B. Barwe, A. Stein, O.E. Cibulka, I. Pelant, J. Ghanbaja, T. Belmonte, J. Benedikt, *Plasma Proc. Polym.* **12** No 2, 132 (2015).
58. V. Medvecká, A. Zahoranová, J. Greguš, D. Kováčik, M. Černák, *WDS'12 Proceedings of Contributed Papers: Part III–Physics*, 58 (Prague: 2012).
59. L. Svandova, A. Groleau, A. Dorval, A. Hamdan, J. Kelar, G. Laroche, J. Profili, *Electrochemical Society Meeting Abstracts 245* (The Electrochemical Society, Inc.: 2024), 1411 (San Francisco, USA: 2024).
60. T. Homola, V. Prysiazhnyi, M. Stupavská, *Int. J. Nanomanufact.* **11** No 5/6, 237 (2015).
61. A. Pamreddy, D. Skácelová, M. Haničinec, P. St'ahel, M. Stupavská, M. Černák, J. Havel, *Surf. Coat. Technol.* **236**, 326 (2013).
62. R. Krumpolec, J. Čech, J. Jurmanová, P. Ďurina, M. Černák, *Surf. Coat. Technol.* **309**, 301 (2017).
63. E.M. Van Veldhuizen, W.R. Rutgers, *Invited paper, Proc. Frontiers in LowTemp. Plasma Diagn. IV*, 40 (Rolduc, Netherlands: 2001).
64. J.-S. Chang, P.A. Lawless, T. Yamamoto, *IEEE Trans. Plasma Sci.* **19** No 6, 1152 (1991).
65. A. De Zanet, M. Salvo, V. Casalegno, *Ceram. Int.* **48** No 16, 23492 (2022).
66. A. Chakravorty, D. Kabiraj, *J. Lumin.* **244**, 118713 (2022).
67. A. Nikolskaya, D. Korolev, A. Mikhaylov, D. Pavlov, A. Sushkov, E. Okulich, A. Chizhova, A. Konakov, P. Yunin, A. Okhapkin, *J. Appl. Phys.* **135** No 21 (2024).
68. P.G. Han, Z.Y. Ma, Z.B. Wang, X. Zhang, *Nanotechnology* **19** No 32, 325708 (2008).

Морфологічні та оптичні властивості кремнієвих мікронаноструктур, індукованих коронним розрядом постійного струму за атмосферного тиску

O. Boudia[1,2], F. Bitam-Megherbi[1,2], M. Mekious[1,2], F. Bouaraba[1,2], M. Megherbi[1]

[1] *Advanced Technologies Laboratory for Electrical Engineering, Tizi-Ouzou, Algeria*
[2] *Mouloud Mammeri University of Tizi-Ouzou, Algeria*

У цій роботі було продемонстровано прогресивну еволюцію поверхневих мікронаноструктур кремнію за допомогою негативного коронного розряду постійного струму за атмосферного тиску в навколишньому повітрі. Морфологію текстурованих багатокристалічних кремнієвих (mc-Si) та монокристалічних кремнієвих (c-Si) пластин спостерігали за допомогою скануючої електронної мікроскопії. Було виявлено, що зі збільшенням тривалості обробки коронним розрядом утворюються різні мікроструктури, такі як мікросфери на пластині mc-Si та мікрошипи зі сферичними кінчиками на пластині c-Si. Поверхневе відбиття виготовлених мікроструктур досліджували за допомогою УФ-ВІС спектрофотометра. Результати показали, що ефект захоплення світла значно посилюється мікроструктурами, що утворюються під час обробки коронною плазмою, що призводить до суттєвого зниження відбиття світла. Поверхневе відбиття в діапазоні довжин хвиль від 200 нм до 1000 нм виявилося меншим за 8 % для текстурованого mc-Si та лише 0,78 % для текстурованого c-Si. Крім того, фотолюмінесцентні властивості мікроструктур виявили червоне зміщення піків випромінювання. Цей ефект може бути корисним для розробки кремнієвих фотоелектричних елементів, оптоелектронних пристроїв та люмінесцентних застосувань.

Ключові слова: Кремній, Морфологія поверхневих мікроструктур, Коронний розряд, Відбивна здатність, Оптичні властивості.